OPEN

NPG Asia Materials (2016) 8, e285; doi:10.1038/am.2016.77
www.nature.com/am

ORIGINAL ARTICLE

High-performance n-type $Yb_xCo_4Sb_{12}$: from partially filled skutterudites towards composite thermoelectrics

Shanyu Wang[1], James R Salvador[2], Jiong Yang[1], Ping Wei[1], Bo Duan[1] and Jihui Yang[1]

The filling fraction limit (FFL) of skutterudites, that is, the complex balance of formation enthalpies among different species, is an intricate but crucial parameter for achieving high thermoelectric performance. In this work, we synthesized a series of $Yb_xCo_4Sb_{12}$ samples with $x = 0.2$–0.6 and systemically studied the FFL of Yb, which is still debated even though this system has been extensively investigated for decades. Our combined experimental efforts of X-ray diffraction, microstructural and quantitative compositional analyses clearly reveal a Yb FFL of ~0.29 in $CoSb_3$, which is consistent with previous theoretical calculations. The excess Yb in samples with $x > 0.35$ mainly form metallic $YbSb_2$ precipitates, significantly raising the Fermi level and thus increasing the electrical conductivity and decreasing the Seebeck coefficient. This result is further corroborated by the numerical calculations based on the Bergman's composite theory, which accurately reproduces the transport properties of the $x > 0.35$ samples based on nominal $Yb_{0.35}Co_4Sb_{12}$ and $YbSb_2$ composites. A maximum *ZT* of 1.5 at 850 K is achieved for $Yb_{0.3}Co_4Sb_{12}$, which is the highest value for a single-element-filled $CoSb_3$. The high *ZT* originates from the high-power factor (in excess of 50 $\mu W\,cm\text{-}K^{-2}$) and low lattice thermal conductivity (well below 1.0 $W\,m\text{-}K^{-1}$). More importantly, the large average *ZTs*, for example, ~1.05 for 300–850 K and ~1.27 for 500–850 K, are comparable to the best values for n-type skutterudites. The high thermoelectric and thermomechanical performances and the relatively low air and moisture sensitivities of Yb make Yb-filled $CoSb_3$, a promising candidate for large-scale power generation applications.

NPG Asia Materials (2016) **8,** e285; doi:10.1038/am.2016.77; published online 1 July 2016

INTRODUCTION

Waste heat recovery from vehicle exhaust or industrial processes based on thermoelectric (TE) technology is an important component of clean and renewable energy for a sustainable future.[1–3] However, the low efficiency of current TE materials along with the complexities and difficulties in system-level engineering still largely prohibit the widespread applications of this technology.[3,4] Skutterudite antimonide is one of the most promising candidates for intermediate temperature TE power generation (500–900 K) owing to the availability of both high-performance n- and p-type compositions within this material class with excellent thermomechanical properties and relatively low-cost and abundant constituent elements (compared with the state-of-the-art Bi_2Te_3 and PbTe).[4–9] Guest filling in the structural nanovoids to form the so-called filled skutterudites (i.e., $R_y(Co,Fe)_4Sb_{12}$, where *R* represents the filler and *y* the filling fraction) is the best strategy for enhancing the TE figure of merit *ZT* as the fillers both act to control carrier concentration and significantly suppress the propagation of heat-carrying phonons.[6,7] Many elements can be partially filled in $CoSb_3$, such as alkali, alkaline earth, rare earth, and group IIIA elements.[10] Among these elements, Yb is one of the most effective fillers to lower lattice thermal conductivity (κ_L) due to its heavy atomic mass and small ionic radius, which result in the lowest rattling frequency of ~42 cm^{-1} in $CoSb_3$.[10,11]

Despite being studied extensively because of its demonstrably good TE properties ($ZT \sim 1.2$–1.4),[11–17] the filling fraction limit (FFL) of Yb has still not been conclusively determined. Various authors have reported substantially different transport properties for a wide range of Yb filling fractions.[11–13,15–18] Shi *et al.*[19] first determined the theoretical FFL of Yb in $CoSb_3$ to be 0.2 using *ab initio* calculations. This was done by considering the competing effects of secondary phases (mainly $YbSb_2$); later, Mei *et al.*[20] calculated the Yb FFL of 0.3 using a similar density functional theory approach. Even large deviations in the experimentally determined Yb FFL have been reported with values ranging from 0.2 to 0.7.[12,15–18,21] These experimental results all seem to indicate a strong dependence on the synthetic conditions, which most likely relates to the temperature dependence of the FFL or thermodynamically controlled chemical reaction processes.[22] Dilley *et al.*[18] experimentally derived a Yb FFL of 0.22 from the lattice parameters vs *nominal* composition, when the samples were synthesized via a combination of induction melting and annealing. Using a non-equilibrium melt-spinning method, Li *et al.*[17] observed a high Yb-filling fraction of 0.28–0.29 (electron probe microanalysis results) for the sample with nominal composition $Yb_{0.3}Co_4Sb_{12+y}$. Later, Salvador *et al.*[16] observed a filling fraction of ~0.25 (electron probe microanalysis results) for the nominal composition $Yb_{0.4}Co_4Sb_{12}$, which was prepared by an induction melting–long-term annealing–sintering technique, although no sample

[1]Materials Science and Engineering Department, University of Washington, Seattle, WA, USA and [2]General Motors Research and Development, Warren, MI, USA
Correspondence: Professor J Yang, Materials Science and Engineering Department, University of Washington, 315 Roberts Hall, Box 352120, Seattle, WA 98195, USA.
E-mail: jihuiy@uw.edu
Received 7 January 2016; revised 13 April 2016; accepted 14 April 2016

with nominal Yb content >0.4 was prepared. Recently, Ren's Group used high-energy ball milling to prepare a series of bulk $Yb_xCo_4Sb_{12}$ and concluded a very high Yb FFL of 0.5 based on X-ray diffraction (XRD) results,[12,15] and He *et al.*[21] extracted an even higher Yb FFL of ~0.68 in $Yb_xCo_4Sb_{12}$ thin films by the *Rietveld* refinements of XRD patterns. Special attention should be paid to the fact that the Yb FFLs determined from many of these previous studies lack sufficient evidence to unambiguously conclude that such high FFLs are true, and none of them show combined experimental results for lattice parameters and experimentally derived Yb compositions as assessed by electron probe microanalysis or energy-dispersive X-ray spectroscopy (EDS). Most recently, Tang *et al.*[22] studied the Yb-Co-Sb ternary phase diagram and argued that Yb FFL is a thermodynamic parameter that depends on the annealing temperature and nominal composition, which could possibly account for some of the FFL discrepancies. In addition, only a few studies have been devoted to the role of excess Yb (e.g., Yb_2O_3) and its effects on the TE transport properties while exceeding the FFL,[23,24] particularly in light of the fact that such excess Yb may form the electrically insulating Yb_2O_3 or other impurity phases such as metallic YbSb or $YbSb_2$.

In the present work, a series of $Yb_xCo_4Sb_{12}$ ($x=0.2$–0.6) samples were synthesized to study the Yb FFL in $CoSb_3$ and the effects that the impurity phases, especially $YbSb_2$, have on the TE transport properties. The polycrystalline samples were prepared by a traditional melting–annealing–sintering technique, where long-term annealing (1 week) was used to achieve thermodynamic equilibrium. By combining the lattice parameter and EDS results, we clearly demonstrate a Yb FFL of ~0.29 in $CoSb_3$, which is consistent with the experimental results of Li *et al.*[17] and theoretical calculations of Mei *et al.*[20] The main secondary phase for samples with $x>0.3$ is metallic $YbSb_2$ precipitates. This secondary phase exerts a significant influence on the TE transport properties, even at small volume fractions, as we will demonstrate. The two-phase Bergman–Fel theory was successfully used to model the transport properties of the samples with large amounts of $YbSb_2$ precipitates ($x>0.35$), which helps identify the discrepancy between the Yb FFL and the monotonic dependence of the electrical transport properties with Yb contents much greater than the FFL. Owing to the optimized power factor and low lattice thermal conductivity, a high ZT of 1.5 can be achieved for the sample with nominal composition $Yb_{0.3}Co_4Sb_{12}$ (EDS derived Yb content ~0.22), which is comparable to the best reported results of n-type skutterudites and outperforms all previous studies of single-element-filled skutterudites.

EXPERIMENTAL PROCEDURE

All samples with stoichiometries of $Yb_xCo_4Sb_{12}$ ($x=0.2$–0.6) were prepared using a conventional induction melting–quenching–annealing–sintering method. High-purity Co powder (99.995%; Alfa Aesar, Ward Hill, MA, USA), Sb shot (99.9999%; Alfa Aesar) and Yb chunks (99.95%; Alfa Aesar) were used as raw materials. The Co powders were further purified and melted into small shots with sizes of 1–5 mm using arc melting (SA-200; MRF, Inc., Allenstown, NH, USA). The purified Co shots were loaded into a BN crucible together with Sb for induction melting three times at ~2000 °C for 30 s under an Ar atmosphere (EQ-SP-25VIM; MTI Corporation, Richmond, CA, USA). The ingots were crushed and loaded into carbon-coated quartz tubes with appropriate amounts of Yb (carefully polished off the surface oxide layer) and Sb in an argon-filled glove-box (Lab Star, Mbraun Corporation, Garching, Germany) and vacuum sealed (10^{-3} Torr). The charged tubes were placed into a box furnace heated to 1000 °C for 5 h, soaked for 24 h and then quenched in ice water. The ingots were ultrasonically cleaned in ethanol for 10 min, dried at 80 °C, vacuum sealed in quartz tubes and then annealed in a box furnace at 750 °C for 168 h. After annealing, the ingots were surface polished, crushed, hand ground into fine powders (<100 μm) and sintered into bulk materials using spark plasma sintering (SPS) at ~650–700 °C and 50 MPa for 5 min. In addition, a single-phase $YbSb_2$ polycrystalline sample was prepared using a combined vacuum melting (900 °C for 10 h) and SPS (500 °C and 40 MPa for 5 min) technique. 1.5–2-mm-thick wafers with diameters of 12.7 mm as well as $3\times3\times12$ and $0.3\times2.5\times8$ mm^3 rectangular bars were cut for TE property evaluation and Hall coefficient measurements.

The phase identity and purity of the bulk samples were determined by powder XRD (D8 Focus X-ray diffraction, Bruker Corporation, Billerica, MA, USA) using the Cu K_α radiation ($\lambda=1.5406$ Å), and the lattice parameters were refined using the full-profile *Rietveld* refinement method in the *FullProf_Suite* software.[25] The backscattered electron images (BSEs) were collected on a TM3000 electron microscope (Hitachi, Tokyo, Japan) equipped with a Bruker EDS. The chemical compositions were determined using a field emission scanning electron microscope equipped with an Oxford EDS (accelerating voltage 20 kV) (Sirion XL30, FEI Corporation, Hillsboro, OR, USA). The electrical conductivity (σ) and Seebeck coefficient (α) were simultaneously measured using a ZEM-3 (Ulvac Riko, Kanagawa, Japan) in a low-pressure helium atmosphere. The thermal conductivity (κ) was calculated from the measured thermal diffusivity (λ), specific heat (C_p) and density (d) using the relationship $\kappa=\lambda C_p d$. The thermal diffusivity λ was assessed by the laser flash method (LFA-457, Netzsch Corporation, Selb, Germany), and specific heat (C_p) was measured by differential scanning calorimetry using sapphire as the reference (404F1, Netzsch Corporation). The measurement temperatures ranged from 300 to 850 K. The uncertainties in the electrical conductivity, Seebeck coefficient, and thermal conductivity are estimated to be ±5%, ±3% and ±10%, respectively. The high-temperature Hall coefficient measurements (300–750 K) were performed on a homemade Hall system equipped with a 2 T electromagnet. The carrier concentration (n_H) and Hall mobility (μ_H) were estimated from the measured Hall coefficient (R_H) and electrical conductivity by the relation $n_H=r/e|R_H|$ (assuming the Hall factor r is 1.0) and $\mu_H=\sigma|R_H|$, respectively.

RESULTS AND DISCUSSION

Yb filling fraction limit and its existing forms in $CoSb_3$

The powder XRD of $Yb_xCo_4Sb_{12}$ ($x=0.2$–0.6) after annealing are shown in Figure 1a, and all the major reflections can be indexed to the body-centered cubic skutterudite phase with space group I*m*-3 (JCPDS no. 65-3144). All samples show a trace amount of Yb_2O_3 phase due to its very low formation energy, but the volume fraction of Yb_2O_3 does not increase with increasing Yb content, as shown in Figure 1b. $YbSb_2$ can be detected in samples with $x>0.4$, and its volume fraction does increase with increasing nominal Yb content. The estimated volume fractions of $YbSb_2$ from the XRD patterns are ~6% and 11% for the $x=0.5$ and 0.6 samples, respectively. The presence of large amounts of the $YbSb_2$ phase in the XRD for the $x\geqslant0.5$ also suggests that the Yb FFL should be <0.5, which can be further verified by examining the lattice parameters as a function of the nominal and measured Yb contents. As shown in Figure 1c, the lattice parameter, a, increases linearly with increasing Yb content for samples with $x\leqslant0.35$, and saturates at a value of ~9.06 Å for those with nominal Yb contents $x>0.35$, indicating that the Yb FFL is <0.35 owing to the existence of Yb-associated impurity phases, such as Yb_2O_3, as shown in Figure 1b. To quantify the Yb FFL, the actual contents of Yb in the skutterudite phases were measured using a high-resolution Oxford EDS. The results are averaged from 10 randomly selected points (~5 μm spot size) in the skutterudite matrix, and the standard deviations of the 10 points are usually within 0.02 (normalized to $Yb_{x'}Co_4Sb_{12+\delta}$, where x' is the measured Yb content), as shown in Table 1. The actual Yb content in the skutterudite matrix, which is lower than the nominal composition, first increases with increasing Yb content and saturates at a Yb content of ~0.29. The lattice parameter also increases linearly with increasing nominal (up to $x\sim0.35$) and actual Yb

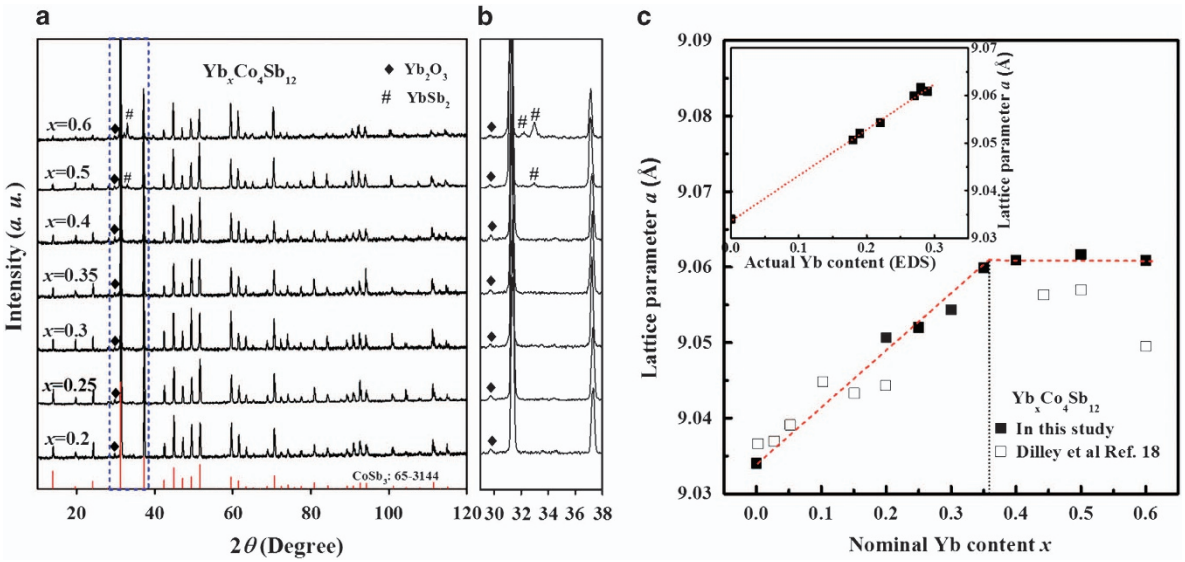

Figure 1 (**a**) Powder X-ray diffraction (XRD) of $Yb_xCo_4Sb_{12}$ after annealing, (**b**) the enlarged XRD highlighting the impurity phases, (**c**) the refined lattice parameter *a* as a function of nominal Yb content *x* for $Yb_xCo_4Sb_{12}$ in this study and previous reported results. The inset in (**c**) shows the lattice parameter as a function of the energy-dispersive X-ray spectrum (EDS)-derived Yb content.

Table 1 Actual Yb content (EDS), ρ, a, n_H, μ_H, η, m^*/m_0 and κ_L at 300 K for $Yb_xCo_4Sb_{12}$ ($x = 0.2$–0.6)

Samples	*Actual Yb content (EDS)*	ρ (*g cm*$^{-3}$)	a (*Å*)	n_H (10^{20} *cm*$^{-1}$)	μ_H (*cm*^{2} *V-s*$^{-1}$)	η	m^*/m_0	κ_L(*W m-K*$^{-1}$)
$x=0.20$	0.18	7.50	9.0401	1.8	57	0.89	2.9	2.4
$x=0.25$	0.19	7.39	9.0461	2.7	50	1.25	3.3	1.9
$x=0.30$	0.22	7.48	9.0502	3.3	44	1.32	3.5	1.9
$x=0.35$	0.27	7.66	9.0521	4.8	36	2.08	3.5	1.8
$x=0.40$	0.28	7.61	9.0562	5.0	35	2.18	3.6	1.7
$x=0.50$	0.28	7.72	9.0626	6.4	32	2.54	3.6	1.7
$x=0.60$	0.29	7.81	9.0609	12	19	3.41	4.4	2.0

Abbreviations: a, lattice parameter; *η*, reduced Fermi energy; EDS, energy-dispersive X-ray spectroscopy; κ_L, lattice thermal conductivity; m_0, free electron mass; m^*, density of states effective mass; μ_H, Hall mobility; n_H, carrier concentration; *ρ*, mass density.

filling fraction (up to ~0.29), as shown in the inset of Figure 1c. These results unambiguously indicate the Yb FFL of ~0.29 in $CoSb_3$, consistent with the theoretical calculations of Mei *et al.*[20] and electron probe microanalysis results of Li *et al.*[17] Notably, the starting stoichiometry, particularly for Sb, or the high annealing temperature may significantly influence the FFL of Yb in $CoSb_3$, as suggested by Tang *et al.*;[22] however, these factors are not applicable in this study as all samples are stoichiometric in Co and Sb and the same annealing temperature was used for every sample.

To further explore the amounts and distributions of the Yb-containing secondary phases (Yb_2O_3 and $YbSb_2$), BSE images were taken from the carefully polished surfaces of SPS'd samples. The advantage of BSE is the ability to provide *Z* contrast to accentuate the presence of Yb-containing impurity phases. Typical BSEs of the $x=0.3$ and 0.5 samples are shown in Figures 2a and b, and the BSEs of the other samples are shown in Supplementary Figure S1 (Supporting Information, SI). The $x<0.35$ samples are approximately pure phase (trace amount of impurities with sizes of ~1 μm), and only minute impurity phases are found for the $x=0.35$ and 0.4 samples. Large amounts of impurity phases with sizes of several micrometers can be observed for the $x=0.5$ and 0.6 samples. Only one kind of impurity phase (white spots) can be identified, and a semiquantitative EDS spectrum taken on a large impurity phase area indicates that the composition is roughly $YbSb_2$ (with significant surface oxidation), as shown in Figures 2c and d. Here, the oxygen in Figure 2d is mainly introduced in the postpolishing and drying processes because of the air and water sensitivity of $YbSb_2$. Elemental mappings of the same area are shown in Supplementary Figure S2. In addition, a semiquantitative analysis of the area fraction of the $YbSb_2$ phase is performed on 10 randomly selected BSE figures (~180×140 μm^2), and the result is shown in Figure 2e. The $x<0.35$ samples show trace amounts of impurity phase (<0.5%, Yb_2O_3 or $YbSb_2$), whereas the impurity content (mainly $YbSb_2$) increases rapidly for the $x\geqslant0.35$ samples, which is consistent with the XRD results showing a saturation in Yb content in the skutterudite matrix. Notably, no Yb_2O_3 phase can be identified in the BSE for any of the samples, most likely due to its small grain size (<1 μm) and small contrast with oxidized $YbSb_2$ in our BSE images. The presence of large amounts of metallic $YbSb_2$ phase, as discussed later, exerts a significant influence on the TE properties, especially for the samples with $x>0.35$.

TE transport properties

The dimensionless figures of merit, *ZT*s, of $Yb_xCo_4Sb_{12}$ ($x=0.2$–0.6) are shown in Figure 3a together with the previous results for some

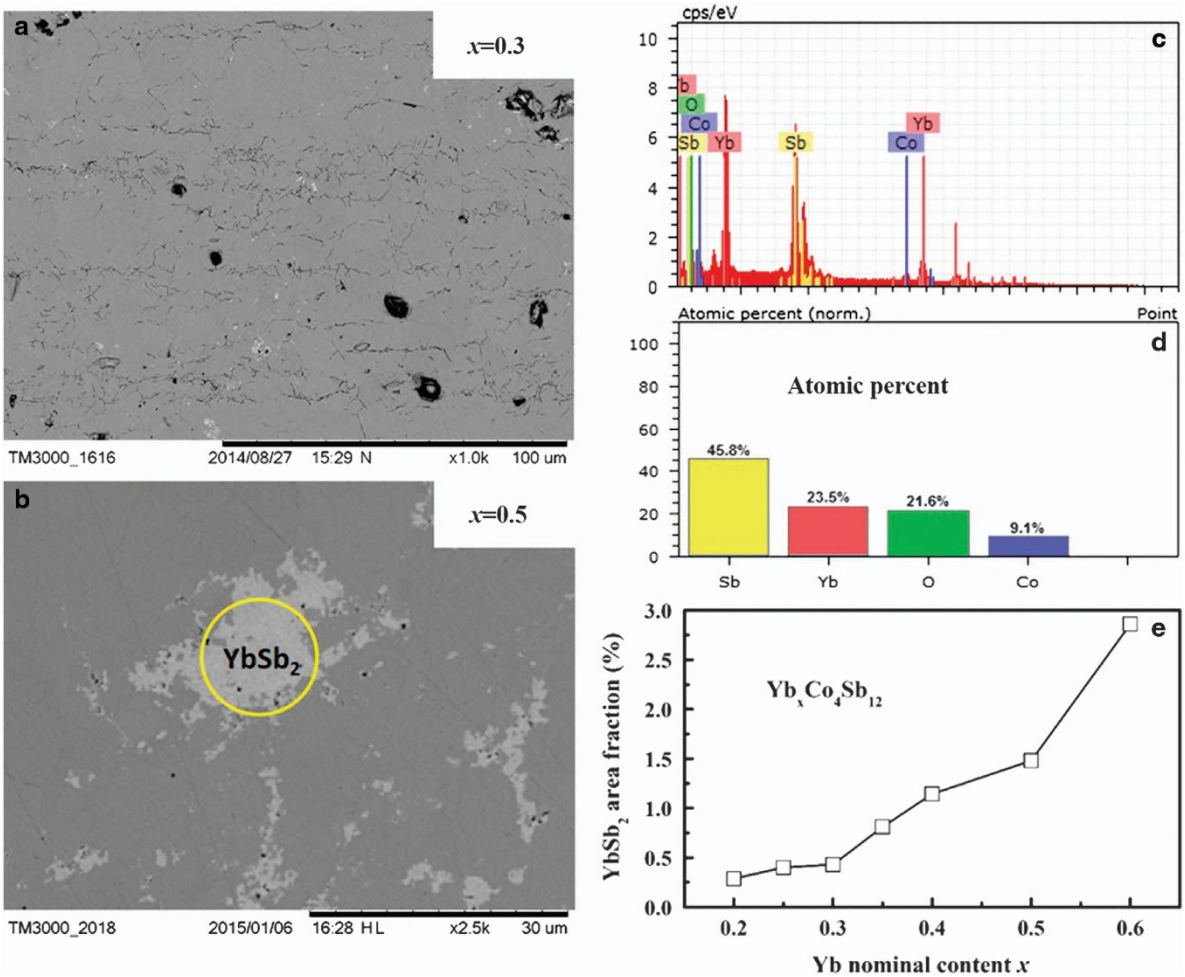

Figure 2 Typical backscattered electron images of (**a**) the $x=0.3$ and (**b**) $x=0.5$ samples, the light color regions in (**b**) is the $YbSb_2$ precipitates; (**c**) energy-dispersive X-ray spectrum (EDS) of the circular area in (**b**); (**d**) quantitative result of the chemical composition from EDS in (**c**); (**e**) the area fraction of $YbSb_2$ precipitates counted from 10 randomly selected scanning electron microscope (SEM) figures (magnification of ×1000).

Yb-filled and the best reported triple-filled $CoSb_3$.[5,12,13,15] Here, ZT is defined as $\sigma\alpha^2T/\kappa$, where α, σ, κ and T are the Seebeck coefficient, electrical conductivity, thermal conductivity and the absolute temperature, respectively. With increasing Yb content, ZT increases gradually, peaks at $x=0.3$ and then decreases rapidly. Our Yb-filled samples show excellent TE performance with a maximum ZT of 1.5 at 850 K for $Yb_{0.3}Co_4Sb_{12}$ (nominal composition), outperforming all previously reported single-element-filled skutterudites,[12,15,17,26–29] and having comparable performance to the best reported values for any n-type skutterudites.[5,8,30] For power generation applications, the average ZT in the temperature range of use is more important to achieve high TE conversion efficiency.[3,31] We therefore compared the average ZTs of $Yb_{0.3}Co_4Sb_{12}$ with those of the best reported ZT of triple-filled $CoSb_3$,[5] as shown in Figure 3b. Even though the $Yb_{0.3}Co_4Sb_{12}$ has a lower peak ZT, it shows comparable average ZT values to those of the best triple-filled $CoSb_3$,[5] specifically $\overline{ZT}_{300-850K} = 1.05$ and $\overline{ZT}_{500-850K} = 1.28$, whereas the relatively lower oxygen and moisture sensitivity of Yb compared with alkali (Li, Na and K), alkaline earth (Ca, Sr and Ba) and other rare earth (La, Ce, Nd and so on) elements make Yb-filled skutterudites more attractive for large-scale synthesis and thus commercial applications. The high TE performance of our Yb-filled $CoSb_3$ is mainly attributed to the high power factors originating from the optimized carrier concentration and high carrier mobility, as well as low lattice thermal conductivity due to the low rattling frequency of Yb (heavy mass and small ionic radius), which will be addressed below in greater detail.

Before presenting the high-temperature transport properties, the room temperature physical properties were analyzed and are summarized in Table 1. With increasing measured Yb content, n_H first increases almost linearly and then rises rapidly for the samples with $x>0.4$. This rapid increase in n_H is most likely attributable to the presence of large amounts of metallic $YbSb_2$ precipitates, as shown in Figure 2 and Supplementary Figure S1. This metallic secondary phase presumably donates electrons into the skutterudite matrix and markedly raises the Fermi level. The n_H values at 300 K, however, are much lower than those estimated by assuming that each Yb donates two electrons, indicated as the dotted line in Supplementary Figure S3. This indicates a complex valence state of Yb and high portion of covalent bonding between Yb and Sb, as evidenced by the low electron-donating ability of Yb ($<1e^-$ per Yb atom at 300 K in Supplementary Figure S3). The intermediate valence of Yb (Yb^{2+}/Yb^{3+}) has been observed for the p-type $YbFe_4Sb_{12}$[32] and $Ce_{1-x}Yb_xFe_4Sb_{12}$,[33] as well as highly charge compensated n-type compositions such as $Yb_yCo_4Sn_xSb_{12-x}$.[18] However, the valence state

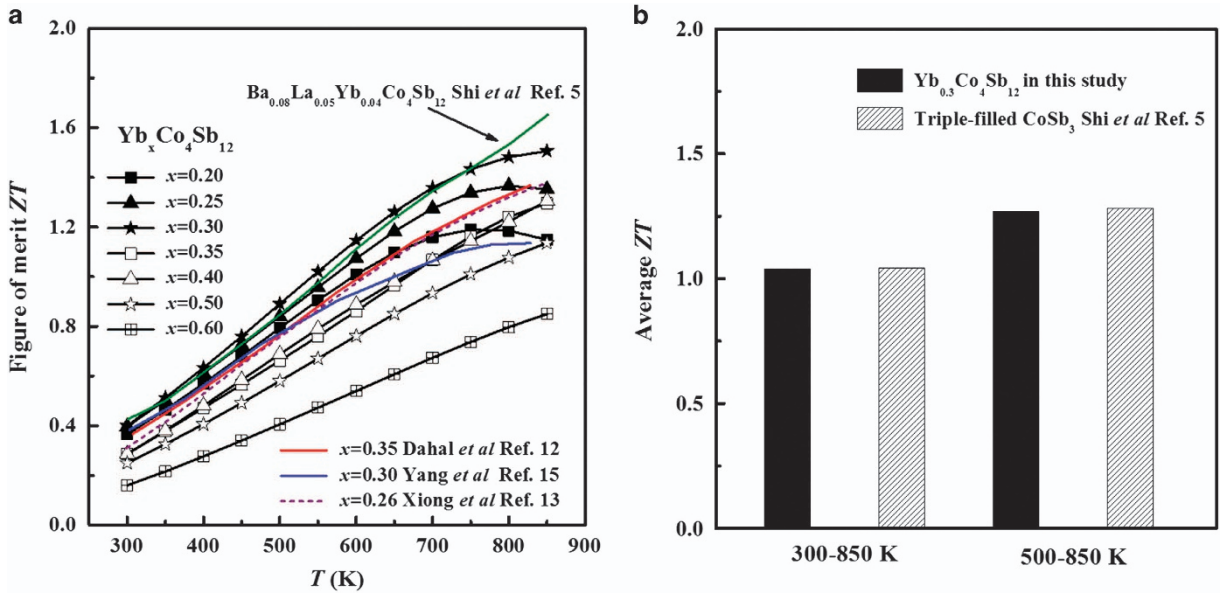

Figure 3 (**a**) Dimensionless figure of merit *ZT* as a function of temperature for $Yb_xCo_4Sb_{12}$ in the present and some previous studies,[12,13,15] and the best triple-filled $CoSb_3$.[5] (**b**) The average *ZT*s of 300–850 and 500–850 K for the best Yb-filled sample in this study and the best triple-filled $CoSb_3$.[5]

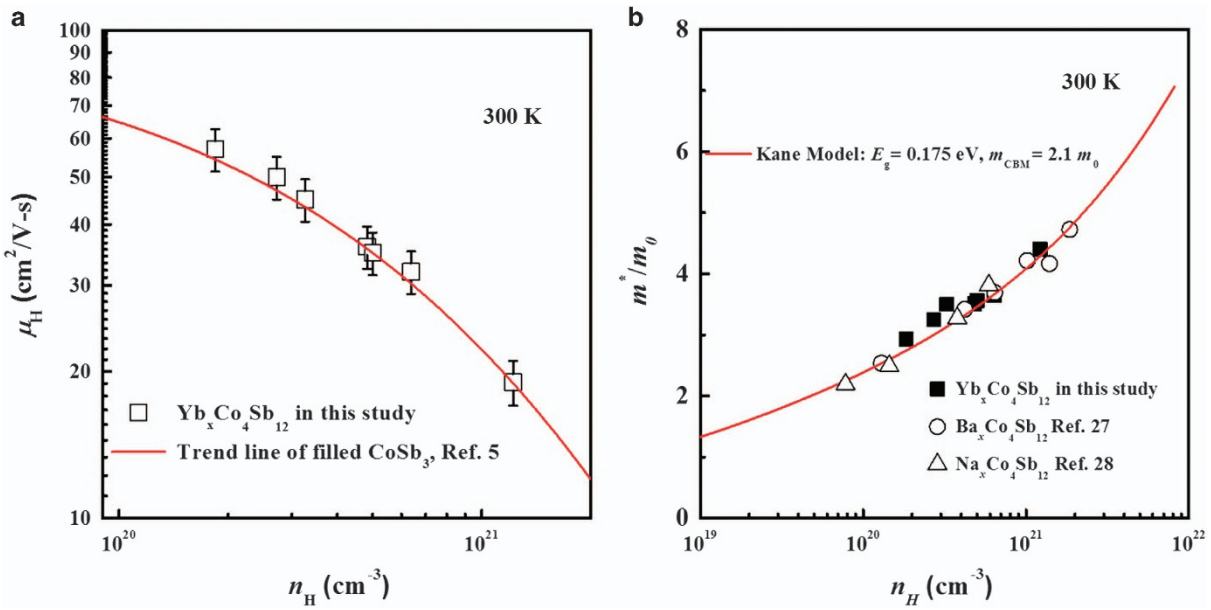

Figure 4 (**a**) Hall mobility as a function of carrier concentration, and the solid line is the trendline of the filled $CoSb_3$. (**b**) Electron effective masses as functions of carrier concentration for $Yb_xCo_4Sb_{12}$ in the present study and Ba- and Na-filled $CoSb_3$;[27,28] the solid line represents the single Kane band model with $E_g = 0.175$ eV and $m_{CBM} = 2.1\ m_0$.

of Yb in non-charge compensated n-type $Yb_xCo_4Sb_{12}$ seems to be well below +2 based on the Hall data and needs to be scrutinized further. With increasing Yb content, μ_H decreases progressively owing to the increased Fermi energy and degeneracy, as shown in Table 1. The μ_H as a function of n_H is plotted in Figure 4a, and the solid line shows the trendline of filled skutterudites (from Shi *et al.* [5]). The μ_H–n_H data for samples presented in this study agree with the trendline, even for the samples with large amounts of $YbSb_2$ precipitates. This implies that the $YbSb_2$ phase has a negligible influence on carrier scattering, most likely due to the band alignment of the two phases or the much smaller electron wavelength (<100 nm for heavily doped semiconductors) compared with the sizes of the $YbSb_2$ precipitates. The negligible influence of $YbSb_2$ on electron scattering is further corroborated by the effective mass m^* vs n_H plots at 300 K, as shown in Figure 4b. The reduced Fermi level η and m^* were calculated using the experimental α and n_H based on the assumption of a single parabolic band and acoustic phonon scattering. The calculation details can be found elsewhere.[34,35] m^* increases gradually with increasing

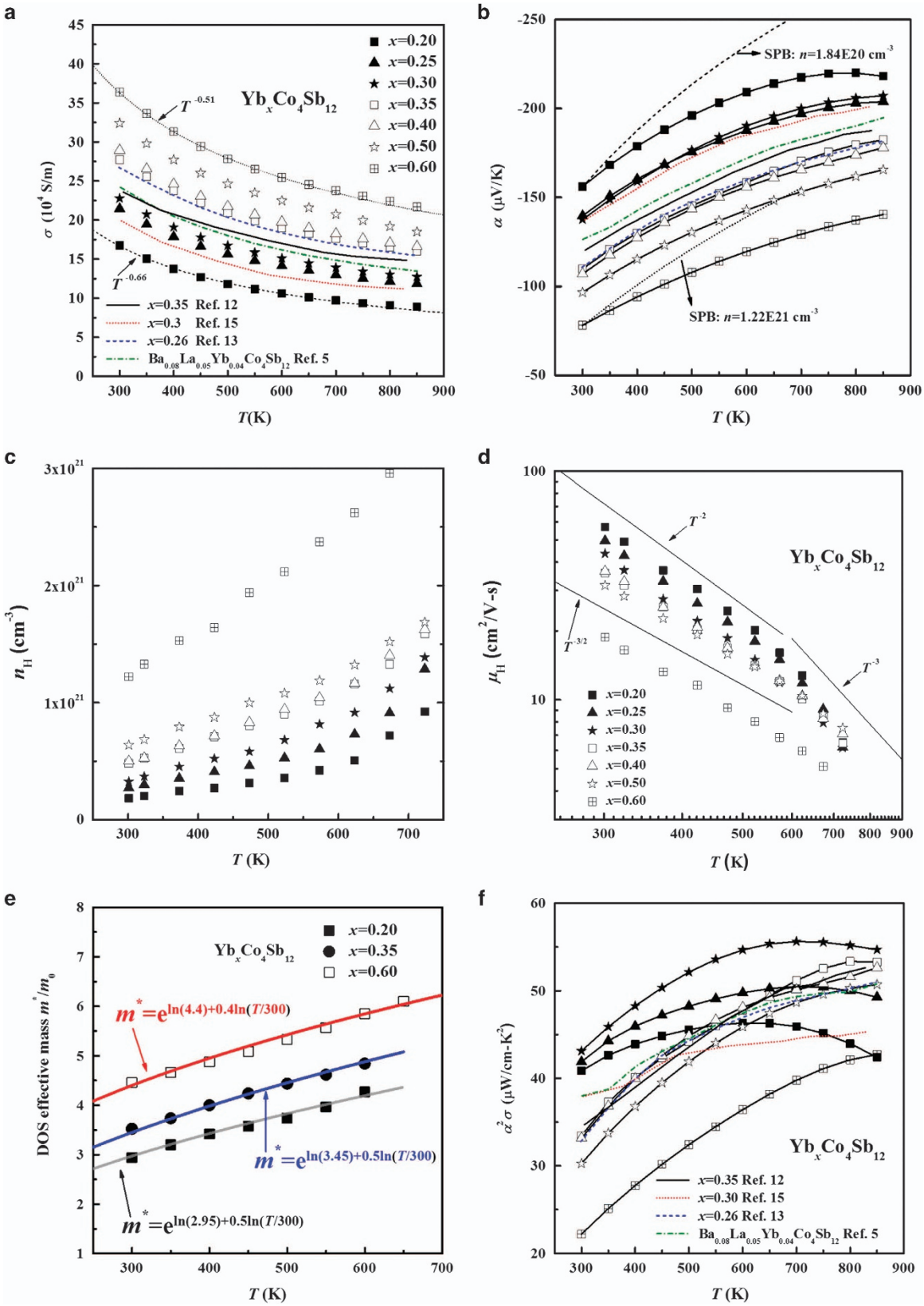

Figure 5 Temperature dependences of the electrical transport properties for $Yb_xCo_4Sb_{12}$ in the present and some previous studies[12,13,15] and the best triple-filled $CoSb_3$.[5] (**a**) Electrical conductivity, (**b**) Seebeck coefficient, (**c**) carrier concentration, (**d**) Hall mobility, (**e**) carrier effective mass and (**f**) power factor.

carrier concentration, consistent with the nonparabolicity of the band edges as found in many previous studies.[5,27,28] The nonparabolic Kane band model describes the effective mass as a function of the reduced Fermi level as

$$m^* = m_{CBM}(1 + \frac{2\eta k_B T}{E_g}), \quad (1)$$

where E_g is the band gap, m_{CBM} the effective mass at the conduction band minimum and k_B the Boltzmann's constant. As shown as the solid line ($m_{CBM} = 2.1m_0$ and $E_g = 0.175$ eV) in Figure 4b, the m^*–n_H relation of Yb-filled $CoSb_3$ in this study agrees well with previous studies of alkaline- or alkaline-earth-filled $CoSb_3$,[27,28] indicating that the $YbSb_2$ precipitates have negligible influence on the carrier scattering, consistent with the μ_H–n_H results. According to the above results, we conclude that for our $Yb_xCo_4Sb_{12}$ samples, even with large amount of metallic $YbSb_2$ precipitates ($x > 0.35$), electron transport is dominated by the conduction band electrons of skutterudites. The $YbSb_2$ precipitates, which donate electrons into the skutterudite matrix, have a negligible influence on the electron scattering, and thus transport. However, the detailed interactions (band alignment, electron transfer, interfacial barrier, and so on) between $YbSb_2$ and skutterudites needs more theoretical and experimental efforts.

The high-temperature (300–850 K) electrical transport properties of $Yb_xCo_4Sb_{12}$ ($x = 0.2$–0.6) and some previously reported results are shown in Figure 5.[5,12,13,15] Electrical conductivity increases gradually with increasing Yb content, as shown in Figure 5a, mainly due to the increased n_H. Notably, the electrical conductivities reported by different authors show a distinct dependence on the nominal Yb content, primarily attributed to the different synthetic techniques, and thus quite different actual Yb filling fractions.[12,13,15–18] The electrical conductivities of all samples obey a power law with temperature ($\sigma \sim T_s$), and the temperature exponent s changes gradually from -0.66 to -0.51 with increasing Yb content. These s values are atypical for heavily doped semiconductors at high temperatures (above the Debye temperature), where σ typically decreases much more rapidly with increasing temperature ($T^{-1.5}$–T^{-2} for lattice scattering), as reported for Bi_2Te_3[36] and PbTe.[37] The unusual temperature dependence of σ can be ascribed to either other carrier scattering mechanisms (e.g., impurity scattering) or the rapid change in n_H with temperature.[29] Furthermore, α decreases gradually with increasing Yb content owing to the increased n_H and thus η, as shown in Figure 5b. The temperature dependence of α is also different from that of conventional heavily doped semiconductors. The experimental data from this study are compared with the calculated values for the $x = 0.2$ (black dashed) and $x = 0.6$ (dotted lines) samples in Figure 5b. These calculated lines are based on the assumptions of temperature-independent carrier concentrations (300 K values of the $x = 0.2$ and $x = 0.6$ samples), a single parabolic band approximation and acoustic phonon scattering.[38] The weak temperature dependences of α and σ indicate unusual electrical transport in Yb-filled $CoSb_3$ compared with typical heavily doped semiconductors, such as Bi_2Te_3[36] and PbTe.[37]

To unravel the underlying reason for the anomalies in the electrical transport, the high-temperature (300–700 K) n_H and μ_H were measured and are shown in Figures 5c and d. Unlike typical extrinsic semiconductors such as doped Bi_2Te_3[36,39] or PbTe,[40] which show weakly temperature-dependent n_H, the n_H of $Yb_xCo_4Sb_{12}$ increases significantly with increasing temperature, which has been widely observed for filled skutterudites.[9,29,41–43] The rapid rise in n_H starting at very low temperatures[41] should be irrelevant to the intrinsic conduction or temperature-dependent solubility of fillers. We speculate that this phenomenon should relate to the unusual temperature dependence of valence state of fillers, which most likely gradually increase their valence states with increasing temperature; this behavior is attributable to the gradual ionization of Yb. This is also corroborated by the weakly temperature-dependent n_H of pristine or doped $CoSb_3$ (Fe, Cr and Te).[44–46] However, more experimental and theoretical work is needed to distinctly address this anomalous temperature dependence of the n_H of filled skutterudites. Moreover, μ_H decreases sharply with increasing temperature (temperature exponent ~ -1.5 to -2), which can be well understood by the nonpolar acoustic phonon scattering and increased m^* with temperature, as shown in Figure 5e. The predominance of acoustic phonon scattering is consistent with many previous studies and typical of good TE compounds at elevated temperatures (higher than the Debye temperature).[13,36,40,47] The temperature exponent of μ_H increases gradually to -3 at 700 K, which is attributable to the increased contribution of optical phonon scattering and/or intensified electron-hole coupling.[48,49] The m^* of selected samples, shown in Figure 5e, increase gradually with temperature. The increase in m^* is mainly due to the lattice expansion and concomitant alterations in band structure, as experimentally observed in many compounds with nonparabolic bands.[40,50,51] The temperature index $d\ln m^*/d\ln T = 0.5$ for the $x < 0.35$ samples is consistent with the result of n-type PbTe,[37,40] which is also well described by the single Kane band model. The $x = 0.6$ sample shows a smaller index of ~ 0.4, presumably due to the influence of the $YbSb_2$ impurity phase and its very large Fermi energy. Based on the above analyses, the unusual temperature-dependent behavior of the electrical transport properties is mainly associated with the rapid increase of n_H with temperature and partly due to the temperature dependence of m^*.

The temperature-dependent power factors ($PF = \alpha^2\sigma$) of $Yb_xCo_4Sb_{12}$ ($x = 0.2$–0.6) and some previously reported values are shown in Figure 5f.[5,12,13,15] With increasing Yb content, the PF first increases and then decreases, reaching a maximum for $Yb_{0.3}Co_4Sb_{12}$ with a highest value of 55 μW cm-K^{-2} at 700 K. More importantly, the high $PF > 50$ μW cm-K^{-2} can be retained over a wide temperature range ($T > 400$ K), which is favorable for achieving a high average ZT. The high PF is superior to previous results for Yb-filled or other single-filled samples and comparable to the best reported results.[5,12,13,15] The high PF is primarily attributed to the optimized carrier concentration and high carrier mobility that originated from the excellent sample purity and uniformity, as demonstrated above.

Temperature-dependent thermal conductivities (κ) of $Yb_xCo_4Sb_{12}$ ($x = 0.2$–0.6) and some previously reported results are shown in Figure 6a.[5,12,13,15] Our Yb-filled samples show slightly higher κ at low temperatures (< 600 K) but comparable values at elevated temperatures to those previously reported Yb-filled $CoSb_3$.[12,13] The differences in low temperature κ are mainly attributed to the difference in microstructure, where the samples in Dahal *et al.*[12] and Xiong *et al.*[13] show nanosize grains (high energy ball milled or in-situ formed), while our samples display grain sizes of tens of micrometers. The triple-filled sample shows much lower κ over the entire temperature range primarily due to the broad-frequency phonon scattering by the multiple filling. However, the specific heat used for the κ calculation in this study is $\sim 10\%$ (~ 0.22 vs ~ 0.24 J g-K^{-1}) higher compared with that of triple-filled sample, as shown in Figure 6b. This could partly account for the difference in κ. The lattice thermal conductivity (κ_L) was calculated by subtracting the

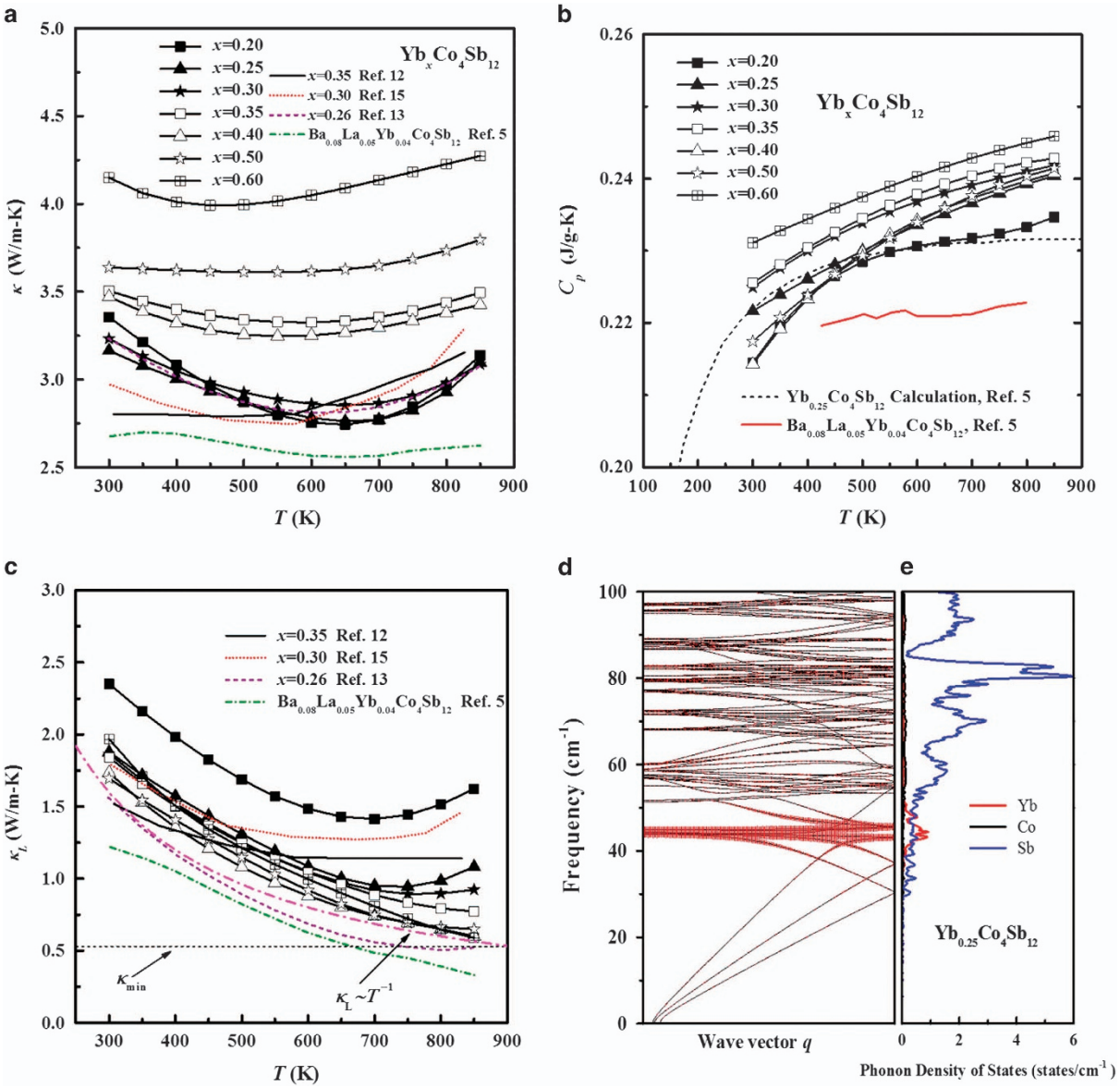

Figure 6 (**a**–**c**) Temperature dependences of the thermal transport properties for $Yb_xCo_4Sb_{12}$ in the present and some previous studies[12,13,15] and best triple-filled $CoSb_3$.[5] (**a**) Thermal conductivity, (**b**) specific heat and (**c**) lattice thermal conductivity. (**d**) Phonon dispersion of and (**e**) partial phonon density of states of $Yb_{0.25}Co_4Sb_{12}$. The red vertical bars superimposed on the phonon dispersion in (**d**) represent the partial contribution from Yb.

carrier contribution from the total thermal conductivity using the formula $\kappa_L = \kappa - L\sigma T$, where L is the Lorenz constant and is taken to be 2.0×10^{-8} V^2 K^{-2} in the present study. Here, the calculated κ_L contains bipolar thermal conductivity at elevated temperatures for the samples with low Yb contents ($x < 0.35$). As shown in Figure 6c, κ_L decreases gradually with increasing actual Yb content (EDS-derived Yb filling fraction) to a minimum value of ~1.7 W m-K^{-1} at 300 K. The $x = 0.6$ sample shows slightly increased κ_L at 300 K, primarily ascribed to the presence of large amounts of $YbSb_2$ precipitates with high thermal conductivity (~15 W m-K^{-1} at 300 K, inset in Figure 7d). At high temperatures, κ_L approaches the minimum value (κ_{min}) of $CoSb_3$,[5] indicating very strong phonon scattering for Yb-filled samples. As shown in Figure 6c, κ_L roughly follows a T^{-1} relation until the involvement of bipolar thermal transport, indicating the predominance of Umklapp processes. As mentioned above, Yb is an indispensable filler for high-performance n-type skutterudites, as indicated for previously reported double- or triple-filled samples.[5,52] Yb-filled $CoSb_3$ actually possesses comparable κ_L values to those of double- or triple-filled $CoSb_3$ considering the experimental error and different C_p used for κ calculations, as shown in Supplementary Figure S4. The intrinsically low κ_L of Yb-filled $CoSb_3$ can be well understood from the specific features of its phonon dispersion, as shown in Figure 6d. Yb-related 'rattling' modes (low-lying optical branches) mainly locate at low frequencies in the range of ~40–45 cm^{-1}, as shown in Figures 6d and e. Such low frequencies are attributable to the small radius and heavy mass of Yb. The low-lying 'rattling' modes interact strongly with the heat-carrying acoustic branches, as characterized by the significant avoided-crossing and low cutoff frequency of the longitudinal acoustic phonon branch.[53] The strong optical–acoustic interactions and possibly intensified anharmonic lattice dynamics are believed to contribute to the very low κ_L, as suggested for numerous TE systems.[54–56] Other fillers, such as Ba and

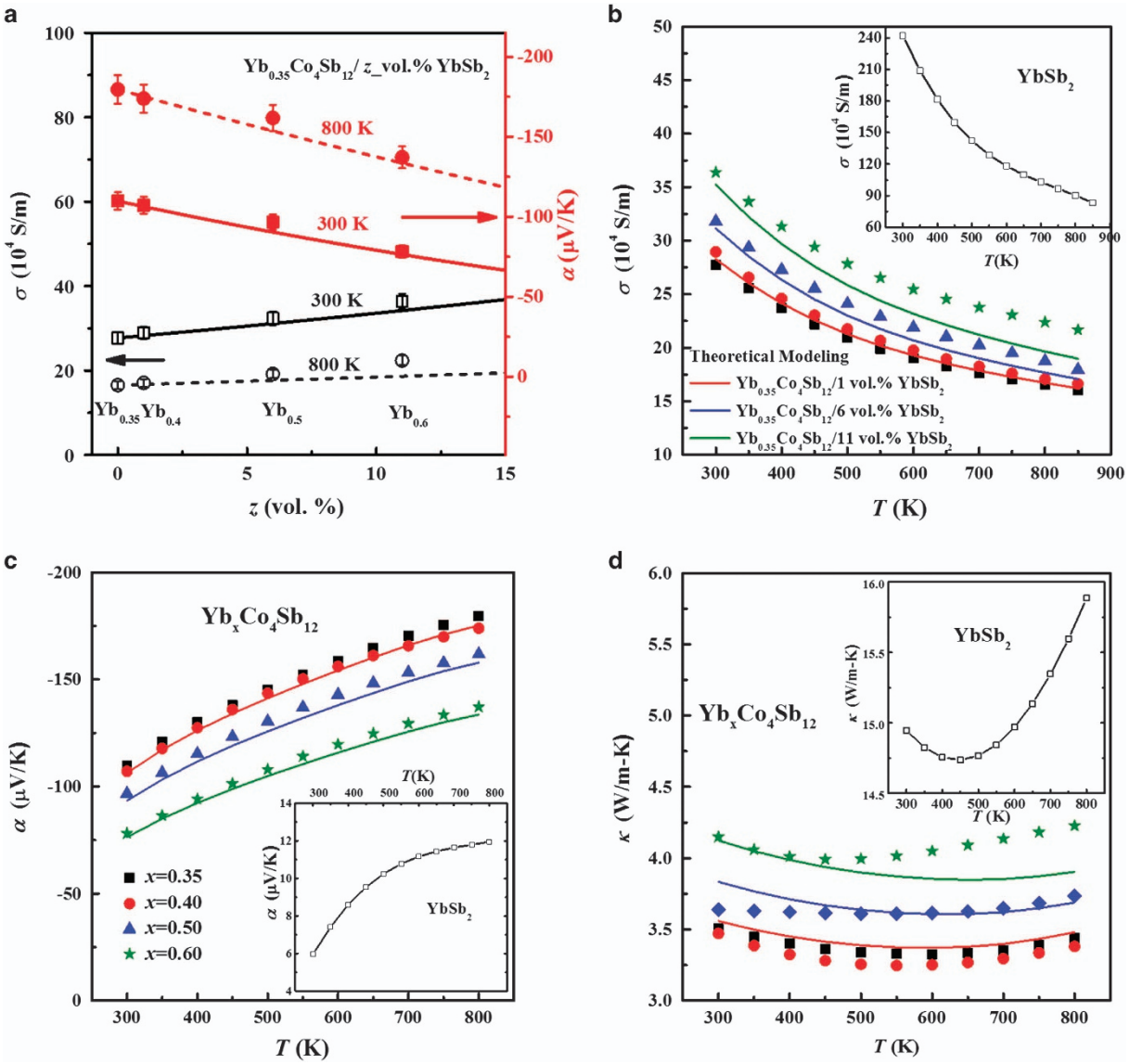

Figure 7 Modeling of the thermoelectric (TE) properties of the $x>0.35$ samples using the Bergman–Fel theory with $Yb_{0.35}Co_4Sb_{12}$/z_vol% $YbSb_2$ composites. (**a**) Electrical conductivity and Seebeck coefficient at 300 and 800 K as functions of $YbSb_2$ volume fraction z; the solid and dashed lines are calculated using the Bergman–Fel theory. The error bars in (**a**) are 5%. Temperature dependences of (**b**) electrical conductivity, (**c**) Seebeck coefficient and (**d**) thermal conductivity for the $x \geqslant 0.35$ samples. The solid lines in (**b**)–(**d**) are theoretical modeling, with $z=1.0$, 6.0 and 11, respectively; the insets in (**b**)–(**d**) are the experimental electrical conductivity, Seebeck coefficient and thermal conductivity of the $YbSb_2$ polycrystalline sample, respectively.

Na(Supplementary Figure S4), have limited effect on κ_L owing to the high frequencies of rattling modes, which show negligible interactions with acoustic branches. In addition, the phonon carrier scattering is another possible contributor to the low κ_L, as suggested in $Co_{1-x}Ni_xSb_3$[57] and La_3Te_4.[58]

TE property modeling of the $x>0.35$ samples using the Bergman–Fel composite theory

The presence of metallic $YbSb_2$ precipitates has significant effects on the TE transport properties of the $x>0.35$ samples, which accounts for the nonlinear dependence of the Yb-filling fraction on carrier concentration and electrical transport. According to the Bergman–Fel model,[59,60] for a system with randomly dispersed component B with spherical shape (namely, $YbSb_2$) in a matrix medium A (namely, $Yb_{0.35}Co_4Sb_{12}$), the effective electrical and thermal conductivities σ_E and κ_E and effective Seebeck coefficient α_E can be estimated from the electrical conductivities σ_A and σ_B, the thermal conductivities κ_A and κ_B and the Seebeck coefficients α_A and α_B of constituents A and B by

$$\sigma_E = \sigma_A + \frac{\Phi}{D}\left(\frac{\delta_\sigma}{d_{BA}} + \frac{1-\Phi\sigma_A}{3\ d_A}\right) \quad (2)$$

$$\kappa_E = \kappa_A + \frac{\Phi}{D}\left(\frac{\delta_\kappa}{d_{BA}} + \frac{1-\Phi\kappa_A}{3\ d_A}\right) \quad (3)$$

$$\alpha_E = \left[\alpha_A\sigma_A + \frac{\Phi}{D}\left(\frac{\delta_{\alpha\sigma}}{d_{BA}} + \frac{1-\Phi\alpha_A\sigma_A}{3\ d_A}\right)\right]\frac{1}{\sigma_E} \quad (4)$$

where Φ is the volume fraction of phase B and

$$\delta_\sigma \equiv \sigma_B - \sigma_A, \quad \delta_\kappa \equiv \kappa_B - \kappa_A, \quad \delta_{\alpha\sigma} \equiv \alpha_B\sigma_B - \alpha_A\sigma_A \tag{5}$$

$$d_A \equiv \frac{\sigma_A\kappa_A}{T} - (\alpha_A\sigma_A)^2, \quad d_{BA} \equiv \frac{\delta_\sigma\delta_\kappa}{T} - \delta_{\alpha\sigma}^2 \tag{6}$$

and

$$D = \left(\frac{\delta_\sigma}{d_{BA}} + \frac{1-\Phi\sigma_A}{3\ d_A}\right)\left(\frac{\delta_\kappa}{Td_{BA}} + \frac{1-\Phi\ \kappa_A}{3\ Td_A}\right) - \left(\frac{\delta_{\alpha\sigma}}{d_{BA}} + \frac{1-\Phi\alpha_A\sigma_A}{3\ d_A}\right)^2 \tag{7}$$

Based on the above equations and TE transport properties of nominal $Yb_{0.35}Co_4Sb_{12}$ and $YbSb_2$, the TE properties of $Yb_{0.35}Co_4Sb_{12}$/*z*_vol% $YbSb_2$ composite (*z* is the volume fraction of $YbSb_2$) can be numerically calculated and are indicated by the solid (300 K) and dashed (800 K) lines in Figure 7. The $YbSb_2$ volume fractions estimated using XRD refinements are ~1, 6 and 11% for the $x = 0.4$, 0.5 and 0.6 samples, respectively. We compared the TE transport properties of $x > 0.35$ samples with the theoretical modeling. Overall, the Bergman–Fel model agrees well with the experimental results, both in magnitude and temperature dependence. As shown in Figure 7a, the electrical conductivity and Seebeck coefficient at 300 and 800 K for the $x > 0.35$ samples agree with the theoretical lines within 5% error. The deviation between the model and experimental data for the $x = 0.6$ sample is relatively large but acceptable considering the simplicity of the model (even distribution and spherical shape of the secondary phase) and system complexity. Owing to the absence of bipolar conduction for the $x > 0.35$ samples (large Fermi energy),[61] the theory also accounts for the temperature dependence of electrical conductivity and Seebeck coefficient, as shown in Figures 7b and c. In particular, the modeled thermal conductivity in Figure 7d shows reasonably good agreement with the experimental data. Because the Bergman–Fel model does not account for carrier or phonon scattering at the phase boundary,[59] the high level of agreement between experimental and modeled electrical and thermal transport properties indicates negligible interfacial scattering between $YbSb_2$ and skutterudites matrix for both electrons and phonons. This is also validated by the high level of agreement for the μ_H–n_H and m^*–n_H data with the general trends of other n-type filled skutterudites shown in Figure 3 and the convergence of κ_L of the $x > 0.35$ samples shown in Figure 6c. Therefore, we can conclude that, for the $x > 0.35$ samples containing micron-sized $YbSb_2$ precipitates, the two-phase Bergman–Fel model can account for the variation in the electrical and thermal transport properties and can unravel the inconsistency between the Yb FFL and the transport properties, as shown for previously reported Yb-filled $CoSb_3$.[12,15]

The best *ZT* is achieved for the pure phase $Yb_{0.3}Co_4Sb_{12}$, and the incorporation of the $YbSb_2$ secondary phase gradually deteriorates the TE performance. This is primarily attributed to the following two causes: (a) the deviation from the optimal carrier concentration range for the $x > 0.3$ samples ($n > 4 \times 10^{19}\ cm^{-3}$) and (b) large size of the $YbSb_2$ precipitates. According to the composites theory,[59] the effective figure of merit of a composite can never exceed the largest figure of merit in any of its constituents in the absence of size and interfacial effects. The large $YbSb_2$ precipitates clearly have no influence on the electron and phonon scattering, which accounts for the decreased *ZT* with increased $YbSb_2$ incorporation. Therefore, to further improve the *ZT*, manipulating the size of $YbSb_2$ (e.g., *in situ* or *ex situ* nanostructuring[62]) to exert strong phonon scattering but negligible electron scattering is necessary, while also retaining the carrier concentration within the optimal range. In the future, rapid solidification (e.g., melt spinning[9,17]) or high-energy ball milling[12] will be used to synthesize the $Yb_yCo_4Sb_{12}/YbSb_2$ nanocomposites to verify this.

CONCLUSIONS

We show in this study that a high *ZT* of 1.5 and a large average $ZT > 1.0$ between 300 and 850 K can be achieved for Yb-filled skutterudites. These are the highest values reported for single-element-filled skutterudites and are comparable to the best reported results for this material class. The high TE performance is primarily attributed to the high power factor (in excess of 50 μW cm-K^{-2} above 400 K) originating from the optimal carrier concentration and superior carrier mobility, as well as the low lattice thermal conductivity due to the significantly modified phonon dispersion from Yb filling. Furthermore, our combined experimental XRD, lattice parameter and EDS results clearly show a Yb FFL of ~0.29, clarifying the long-standing debate. We find that excess Yb mainly forms metallic $YbSb_2$ precipitates, further increasing the electrical conductivity and decreasing the Seebeck coefficient significantly by considerably increasing the overall carrier concentration. The transport properties of the $x > 0.35$ samples with large amounts of $YbSb_2$ precipitates can be quantitatively modeled by Bergman's composite theory ($Yb_{0.35}Co_4Sb_{12}/YbSb_2$ composites), providing new understanding of the role of Yb and its secondary phases in $CoSb_3$, as well as its effects on TE properties. The high TE performance and low preparation cost of Yb-filled $CoSb_3$ make it a promising candidate for large-scale intermediate temperature power generation applications.

CONFLICT OF INTEREST

The authors declare no conflict of interest.

ACKNOWLEDGEMENTS

We thank Dr Feiyue Ma and Prof. Jiangyu Li in the Mechanical Engineering Department at the University of Washington for the kind help in the high temperature Hall measurements. This work was supported by the US Department of Energy under corporate agreement DE-EE0005432, by GM, and by the National Science Foundation under award number 1235535.

Author contributions: SW, PW and BD synthesized the samples and carried out the measurements of the TE properties. JRS performed the X-ray Rietveld analyses. JY carried out the phonon dispersion calculations. SW and JY conceived the experiments and analyzed the results. SW, JRS and JY wrote the manuscript, and all authors participated in editing.

1 Gur, I., Sawyer, K. & Prasher, R. Searching for a better thermal battery. *Science* **335**, 1454–1455 (2012).
2 Chu, S. & Majumdar, A. Opportunities and challenges for a sustainable energy future. *Nature* **488**, 294–303 (2012).
3 Yang, J. & Caillat, T. Thermoelectric materials for space and automotive power generation. *MRS Bull.* **31**, 224–229 (2006).
4 Salvador, J. R., Cho, J. Y., Ye, Z., Moczygemba, J. E., Thompson, A. J., Sharp, J. W., Koenig, J. D., Maloney, R., Thompson, T., Sakamoto, J., Wang, H. & Wereszczak, A. A. Conversion efficiency of skutterudite-based thermoelectric modules. *Phys. Chem. Chem. Phys.* **16**, 12510–12520 (2014).
5 Shi, X., Yang, J., Salvador, J. R., Chi, M., Cho, J. Y., Wang, H., Bai, S., Yang, J., Zhang, W. & Chen, L. Multiple-filled skutterudites: high thermoelectric figure of merit through separately optimizing electrical and thermal transports. *J. Am. Chem. Soc.* **133**, 7837–7846 (2011).
6 Uher, C. Skutterudites: prospective novel thermoelectrics. *Semicond.d Semimet.* **69**, 139–253 (2001).
7 Nolas, G., Morelli, D. & Tritt, T. M. Skutterudites: a phonon-glass-electron crystal approach to advanced thermoelectric energy conversion applications. *Annu. Rev. Mater. Sci.* **29**, 89–116 (1999).
8 Rogl, G., Grytsiv, A., Rogl, P., Bauer, E., Hochenhofer, M., Anbalagan, R., Mallik, R. & Schafler, E. Nanostructuring of p-and n-type skutterudites reaching figures of merit of approximately 1.3 and 1.6, respectively. *Acta Mater.* **76**, 434–448 (2014).
9 Tan, G., Liu, W., Wang, S., Yan, Y., Li, H., Tang, X. & Uher, C. Rapid preparation of $CeFe_4Sb_{12}$ skutterudite by melt spinning: rich nanostructures and high thermoelectric performance. *J. Mater. Chem. A* **1**, 12657–12668 (2013).

10 Shi, X., Bai, S., Xi, L., Yang, J., Zhang, W., Chen, L. & Yang, J. Realization of high thermoelectric performance in n-type partially filled skutterudites. *J. Mater. Res.* **26**, 1745–1754 (2011).
11 Nolas, G., Kaeser, M., Littleton, R. IV & Tritt, T. High figure of merit in partially filled ytterbium skutterudite materials. *Appl. Phys. Lett.* **77**, 1855–1857 (2000).
12 Dahal, T., Jie, Q., Joshi, G., Chen, S., Guo, C., Lan, Y. & Ren, Z. Thermoelectric property enhancement in Yb-doped n-type skutterudites $Yb_xCo_4Sb_{12}$. *Acta Mater.* **75**, 316–321 (2014).
13 Xiong, Z., Chen, X., Huang, X., Bai, S. & Chen, L. High thermoelectric performance of $Yb_{0.26}Co_4Sb_{12}$/yGaSb nanocomposites originating from scattering electrons of low energy. *Acta Mater.* **58**, 3995–4002 (2010).
14 Dimitrov, I. K., Manley, M. E., Shapiro, S. M., Yang, J., Zhang, W., Chen, L., Jie, Q., Ehlers, G., Podlesnyak, A. & Camacho, J. Einstein modes in the phonon density of states of the single-filled skutterudite $Yb_{0.2}Co_4Sb_{12}$. *Phys. Rev. B* **82**, 174301 (2010).
15 Yang, J., Hao, Q., Wang, H., Lan, Y., He, Q., Minnich, A., Wang, D., Harriman, J., Varki, V. & Dresselhaus, M. Solubility study of Yb in n-type skutterudites $Yb_xCo_4Sb_{12}$ and their enhanced thermoelectric properties. *Phys. Rev. B* **80**, 115329 (2009).
16 Salvador, J., Yang, J., Shi, X., Wang, H., Wereszczak, A., Kong, H. & Uher, C. Transport and mechanical properties of Yb-filled skutterudites. *Philos. Mag.* **89**, 1517–1534 (2009).
17 Li, H., Tang, X., Zhang, Q. & Uher, C. Rapid preparation method of bulk nanostructured $Yb_{0.3}Co_4\ Sb1_{2+y}$ compounds and their improved thermoelectric performance. *Appl. Phys. Lett.* **93**, 252109–252103 (2008).
18 Dilley, N., Bauer, E., Maple, M. & Sales, B. Thermoelectric properties of chemically substituted skutterudites $Yb_yCo_4Sn_xSb_{12-x}$. *J. Appl. Phys.* **88**, 1948–1951 (2000).
19 Shi, X., Zhang, W., Chen, L. & Yang, J. Filling fraction limit for intrinsic voids in crystals: doping in skutterudites. *Phys. Rev. Lett.* **95**, 185503 (2005).
20 Mei, Z., Zhang, W., Chen, L. & Yang, J. Filling fraction limits for rare-earth atoms in $CoSb_3$: an *ab initio* approach. *Phys. Rev. B* **74**, 153202 (2006).
21 He, C., Daniel, M., Grossmann, M., Ristow, O., Brick, D., Schubert, M., Albrecht, M. & Dekorsy, T. Dynamics of coherent acoustic phonons in thin films of $CoSb_3$ and partially filled $Yb_xCo_4Sb_{12}$ skutterudites. *Phys. Rev. B* **89**, 174303 (2014).
22 Tang, Y., Chen, S-w & Snyder, G. J. Temperature dependent solubility of Yb in Yb–$CoSb_3$ skutterudite and its effect on preparation, optimization and lifetime of thermoelectrics. *J. Materiomics* **1**, 75–84 (2015).
23 Zhao, X., Shi, X., Chen, L., Zhang, W., Bai, S., Pei, Y. & Goto, T. Synthesis of $Yb_yCo_4Sb_{12}/Yb_2O_3$ composites and their thermoelectric properties. *Appl. Phys. Lett.* **89**, 92121–92121 (2006).
24 Ding, J., Gu, H., Qiu, P., Chen, X., Xiong, Z., Zheng, Q., Shi, X. & Chen, L. Creation of Yb_2O_3 nanoprecipitates through an oxidation process in bulk yb-filled skutterudites. *J. Electron. Mater.* **42**, 382–388 (2013).
25 Rodríguez-Carvajal, J. Recent advances in magnetic structure determination by neutron powder diffraction. *Phys. B* **192**, 55–69 (1993).
26 Zhao, X., Shi, X., Chen, L., Zhang, W., Zhang, W. & Pei, Y. Synthesis and thermoelectric properties of Sr-filled skutterudite $Sr_yCo_4\ Sb_{12}$. *J. Appl. Phys.* **99**, 053711-053711-053714 (2006).
27 Chen, L., Kawahara, T., Tang, X., Goto, T., Hirai, T., Dyck, J. S., Chen, W. & Uher, C. Anomalous barium filling fraction and n-type thermoelectric performance of Ba_y-Co_4Sb_{12}. *J. Appl. Phys.* **90**, 1864–1868 (2001).
28 Pei, Y., Yang, J., Chen, L., Zhang, W., Salvador, J. & Yang, J. Improving thermoelectric performance of caged compounds through light-element filling. *Appl. Phys. Lett.* **95**, 042101 (2009).
29 Wang, S., Yang, J., Wu, L., Wei, P., Zhang, W. & Yang, J. On Intensifying carrier impurity scattering to enhance thermoelectric performance in Cr-doped $Ce_yCo_4Sb_{12}$. *Adv. Funct. Mater.* **25**, 6660–6670 (2015).
30 Li, H., Tang, X., Zhang, Q. & Uher, C. High performance $In_xCe_yCo_4Sb_{12}$ thermoelectric materials with in situ forming nanostructured InSb phase. *Appl. Phys. Lett.* **94**, 102114 (2009).
31 Bell, L. E. Cooling, heating, generating power, and recovering waste heat with thermoelectric systems. *Science* **321**, 1457–1461 (2008).
32 Dilley, N., Freeman, E., Bauer, E. & Maple, M. Intermediate valence in the filled skutterudite compound $YbFe_4Sb_{12}$. *Phys. Rev. B* **58**, 6287 (1998).
33 Bérardan, D., Godart, C., Alleno, E. & Bauer, E. Chemical properties and thermopower of the new series of skutterudite $Ce_{1-p}Yb_pFe_4Sb_{12}$. *J. Alloy. Compd.* **351**, 18–23 (2003).
34 Wang, S., Tan, X., Tan, G., She, X., Liu, W., Li, H., Liu, H. & Tang, X. The realization of a high thermoelectric figure of merit in Ge-substituted β-Zn_4Sb_3 through band structure modification. *J. Mater. Chem.* **22**, 13977–13985 (2012).
35 Nolas, G. S., Sharp, J. & Goldsmid, J *Thermoelectrics: Basic Principles and New Materials Developments* Vol. 45, (Springer, Berlin, Germany, 2001).
36 Wang, S., Tan, G., Xie, W., Zheng, G., Li, H., Yang, J. & Tang, X. Enhanced thermoelectric properties of $Bi_2(Te_{1-x}Se_x)_3$-based compounds as n-type legs for low-temperature power generation. *J. Mater. Chem.* **22**, 20943–20951 (2012).
37 Pei, Y., LaLonde, A. D., Wang, H. & Snyder, G. J. Low effective mass leading to high thermoelectric performance. *Energy Environ. Sci.* **5**, 7963–7969 (2012).
38 Fistul, V. I*Heavily Doped Semiconductors*, (Plenum Press, New York, NY, USA, 1969).
39 Xie, W., He, J., Kang, H. J., Tang, X., Zhu, S., Laver, M., Wang, S., Copley, J. R., Brown, C. M. & Zhang, Q. Identifying the specific nanostructures responsible for the high thermoelectric performance of $(Bi,Sb)_2Te_3$ nanocomposites. *Nano Lett.* **10**, 3283–3289 (2010).
40 Pei, Y., Gibbs, Z. M., Gloskovskii, A., Balke, B., Zeier, W. G. & Snyder, G. J. Optimum carrier concentration in n-type PbTe thermoelectrics. *Adv. Energy Mater.* **4** (2014).
41 Ballikaya, S., Uzar, N., Yildirim, S., Salvador, J. R. & Uher, C. High thermoelectric performance of In, Yb, Ce multiple filled $CoSb_3$ based skutterudite compounds. *J. Solid State Chem.* **193**, 31–35 (2012).
42 Liu, R., Yang, J., Chen, X., Shi, X., Chen, L. & Uher, C. p-Type skutterudites $R_xM_yFe_3CoSb_{12}$(R,M = Ba, Ce, Nd, and Yb): effectiveness of double-filling for the lattice thermal conductivity reduction. *Intermetallics* **19**, 1747–1751 (2011).
43 Cho, J. Y., Ye, Z., Tessema, M., Waldo, R., Salvador, J. R., Yang, J., Cai, W. & Wang, H. Thermoelectric properties of p-type skutterudites $Yb_xFe_{3.5}Ni_{0.5}Sb_{12}$ ($0.8<x<1$). *Acta Mater.* **60**, 2104–2110 (2012).
44 Yang, J., Meisner, G., Morelli, D. & Uher, C. Iron valence in skutterudites: transport and magnetic properties of $Co_{1-x}Fe_xSb_3$. *Phys. Rev. B* **63**, 014410 (2000).
45 Yang, J., Endres, M. & Meisner, G. Valence of Cr in skutterudites: electrical transport and magnetic properties of Cr-doped $CoSb_3$. *Phys. Rev. B* **66**, 014436 (2002).
46 Li, X., Chen, L., Fan, J., Zhang, W., Kawahara, T. & Hirai, T. Thermoelectric properties of Te-doped $CoSb_3$ by spark plasma sintering. *J. Appl. Phys.* **98**, 083702–083706 (2005).
47 Slack, G. A. & Hussain, M. A. The maximum possible conversion efficiency of silicon-germanium thermoelectric generators. *J. Appl. Phys.* **70**, 2694–2718 (1991).
48 Morin, F. & Maita, J. Electrical properties of silicon containing arsenic and boron. *Phys. Rev* **96**, 28 (1954).
49 Su, X., Li, H., Wang, G., Chi, H., Zhou, X., Tang, X., Zhang, Q. & Uher, C. Structure and transport properties of double-doped $CoSb_{2.75}Ge_{0.25-x}Te_x$ ($x=0.125$–0.20) with *in situ* nanostructure. *Chem. Mater.* **23**, 2948–2955 (2011).
50 Zhitinskaya, M., Kaidanov, V. & Chernik, I. Nonparabolicity of the conduction band of lead telluride. *Sov. Phys. Solid. State* **8**, 246–247 (1966).
51 Lyden, H. A. Temperature dependence of the effective masses in PbTe. *Phys. Rev.* **135**, A514 (1964).
52 Shi, X., Kong, H., Li, C.-P., Uher, C., Yang, J., Salvador, J., Wang, H., Chen, L. & Zhang, W. Low thermal conductivity and high thermoelectric figure of merit in n-type $Ba_xYb_yCo_4Sb_{12}$
double-filled skutterudites. *Appl. Phys. Lett.* **92**, 182101 (2008).
53 Wang, S., Yang, J., Wu, L., Wei, P., Yang, J., Zhang, W. & Grin, Y. Anisotropic multicenter bonding and high thermoelectric performance in electron-poor CdSb. *Chem. Mater.* **27**, 1071–1081 (2015).
54 Christensen, M., Abrahamsen, A. B., Christensen, N. B., Juranyi, F., Andersen, N. H., Lefmann, K., Andreasson, J., Bahl, C. R. & Iversen, B. B. Avoided crossing of rattler modes in thermoelectric materials. *Nat. Mater.* **7**, 811–815 (2008).
55 Lee, S., Esfarjani, K., Luo, T., Zhou, J., Tian, Z. & Chen, G. Resonant bonding leads to low lattice thermal conductivity. *Nat. Commun.* **5**, 3525–3533 (2014).
56 Zhang, Y., Ke, X., Kent, P. R., Yang, J. & Chen, C. Anomalous lattice dynamics near the ferroelectric instability in PbTe. *Phys. Rev. Lett.* **107**, 175503 (2011).
57 Yang, J., Morelli, D., Meisner, G., Chen, W., Dyck, J. & Uher, C. Influence of electron-phonon interaction on the lattice thermal conductivity of $Co_{1-x}Ni_xSb_3$. *Phys. Rev. B* **65**, 094115 (2002).
58 May, A. F., Flage-Larsen, E. & Snyder, G. J. Electron and phonon scattering in the high-temperature thermoelectric $La_3Te_{4-z}M_z$ (M = Sb, Bi). *Phys. Rev. B* **81**, 125205 (2010).
59 Bergman, D. J. & Levy, O. Thermoelectric properties of a composite medium. *J. Appl. Phys.* **70**, 6821–6833 (1991).
60 Xie, W., He, J., Zhu, S., Su, X., Wang, S., Holgate, T., Graff, J., Ponnambalam, V., Poon, S. & Tang, X. Simultaneously optimizing the independent thermoelectric properties in (Ti,Zr,Hf)(Co,Ni)Sb alloy by *in situ* forming InSb nanoinclusions. *Acta Mater.* **58**, 4705–4713 (2010).
61 Wang, S., Yang, J., Toll, T., Yang, J., Zhang, W. & Tang, X. Conductivity-limiting bipolar thermal conductivity in semiconductors. *Sci. Rep.* **5**, 10136 (2015).
62 Li, J.-F., Liu, W.-S., Zhao, L.-D. & Zhou, M. High-performance nanostructured thermoelectric materials. *NPG Asia Mater.* **2**, 152–158 (2010).

Supplementary Information accompanies the paper on the NPG Asia Materials website (http://www.nature.com/am)